

KEK Proceedings 2017-4  
October 2017  
R

# Proceedings of the Twenty-Fourth EGS Users' Meeting in Japan

August 7 - 8, 2017.  
KEK, Tsukuba, Japan

Edited by

Y. Namito, H.Iwase and H. Hirayama



High Energy Accelerator Research Organization

**High Energy Accelerator Research Organization (KEK), 2017**

KEK Reports are available from:

High Energy Accelerator Research Organization (KEK)  
1-1 Oho, Tsukuba-shi  
Ibaraki-ken, 305-0801  
JAPAN

Phone: +81-29-864-5137  
Fax: +81-29-864-4604  
E-mail: [irdpub@mail.kek.jp](mailto:irdpub@mail.kek.jp)  
Internet: <http://www.kek.jp>

## FOREWARD

The Twenty-fourth EGS Users' Meeting in Japan was held at High Energy Accelerator Research Organization (KEK) from August 7 to 8. The meeting has been hosted by the Radiation Science Center. More than 30 participants attended the meeting.

The meeting was divided into two parts. Short course on EGS was held at the first half of the workshop using EGS5 code. In the later half, 4 talks related EGS were presented. The talk covered the wide fields, like the medical application and the calculation of various detector responses *etc.* These talks were very useful to exchange the information between the researchers in the different fields.

Finally, we would like to express our great appreciation to all authors who have prepared manuscript quickly for the publication of this proceedings.

Yoshihito Namito  
Hiroshi Iwase  
Hideo Hirayama  
Radiation Science Center  
KEK, High Energy Accelerator Research Organization

## CONTENTS

<b>Running EGS5 on Raspberry Pi</b>	1
<i>S. Tsuji</i>	
<b>Follow Up on Beta Ray Library for EGS5</b>	7
<i>Y. Namito and H. Hirayama</i>	
<b>Evaluation of Multi-Layered Shielding Materials Based on Analysys of Characteristic X-ray</b>	12
<i>D. Kawahara, T. Tobusawa, and N. Sakurai</i>	

# Running EGS5 with Raspberry Pi

S. TSUJI

*Kawasaki Medical School, Kurashiki 701-0192, Japan*

## Abstract

Raspberry Pi is a single board computer with an ARM processor developed in the UK by the Raspberry Pi Foundation. The latest version is Raspberry Pi 3 Model B, and the installed CPU is ARM Cortex-A 53 which has quad core performance with a clock frequency of 1.2 GHz. As for OS, there is a unique Linux distribution called Raspbian, which can be written to microSD card and used. The fact that Linux can be used means that EGS5 can be executed. I describe the concrete method of EGS5 execution on Raspberry Pi and its computational ability.

## 1 Introduction

Raspberry Pi is a single board computer with an ARM processor developed in the UK by the Raspberry Pi Foundation. The specifications of the latest version of Raspberry Pi 3 model B are quad-core ARM Cortex-A 53 with a clock frequency of 1.2 GHz, loaded with 1 GB RAM. The storage is a microSD card. By burning into this microSD card, you can use the Linux distribution Raspbian, Ubuntu, and even Windows 10. In this time, I downloaded the “Raspbian Jessie” image file from the site of <https://www.raspberrypi.org/downloads/raspbian/> and ran EGS5. In this paper, I describe the construction method of EGS5 with Raspberry pi and the comparison of the calculations with Raspbian on Raspberry Pi and Linux on IBM PC compatible.

## 2 Construction method of EGS5 with Raspberry Pi

First, download “Raspbian Jessie” image from the site “<https://www.raspberrypi.org/downloads/raspbian/>” and burn it to microSD card. After inserting the microSD card, turn on the power, set the network, execute the following command [1].

```
sudo apt-get update
sudo apt-get upgrade
sudo rpi-update
```

In order to run EGS5, Fortran is necessary, so install gfortran 4.9 from “Add / Remove Software” in the GUI environment. Download `egs5.XXXXXX.tar.gz` from the EGS5 site [2] and deploy it. Pass the path to the `egs5/` directory. In `egs5run`, arrange environment such as BASKET. Specify `gfortran` for COMPILER. The special thing to note in order to display the calculation execution time is to rewrite `#!/bin/sh` to `#!/bin/bash`.

Raspberry Pi 3 model B has only 1 GB RAM, so you need to rewrite the parameters of `egs5/include/egs5_h` as follows.

```
parameter (NBFIT = 2)
parameter (NEXFIT = 2)
```

With the above setting, EGS5 can be executed on Raspberry Pi (in Fig 1).

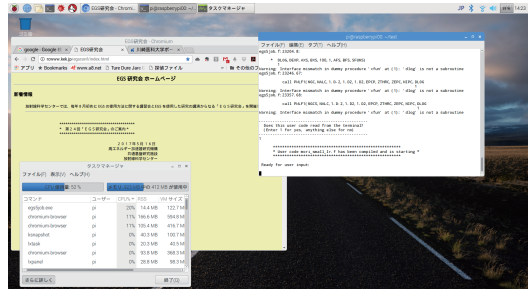


Figure 1: Running EGS5 with Raspberry Pi.

### 3 Construction method of MPI (EGS5-MPI) with Raspberry Pi

Raspberry Pi's Raspbian can run MPI (Message Passing Interface). Download the source code of mpich 3.2 from the site of <https://www.mpich.org/> and expand it. Execute the following command.

```
% configure --prefix=/usr/local/mpich-3.2
% make -j4
% sudo make install
```

If you add `/usr/local/mpich-3.2/bin` to path you can use MPI. EGS5-MPI of EGS5 using MPI can be distributed by e-mail after inquiring [3]. After expanding EGS5-MPI, edit `egs5mpirun` as follows.

```
#!/bin/bash
.....

BASKET=directry of egs5
MPI_BASKET=directry of egs5mpi
MY_MACHINE=MPICH
OPT_LEVEL=02
MPI_SIZE=4
.....

elif test "$MY_MACHINE" = "MPICH" <-- change where "Cygwin MPICH2" is written
.....
CFLAGS="-fno-automatic -finit-local-zero -fno-range-check"
```

With the above setting, EGS5-MPI (`egs5mpirun`) can be executed.

### 4 Comparison of the calculations with Raspberry Pi and IBM PC compatible

I compared the computing power of Raspberry Pi with IBM PC compatible. The program used is `ucsource.f` (in Fig. 2) which is posted on the site [4] and `test_small_Ir.f` (in Fig. 3) which I made [5]. With regard to `ucsource.f`, it is just to emit photons linearly, and for `test_small_Ir.f`, the absorbed dose in water using the microSelectron HDR-v2 is obtained.

The specifications of the IBM PC compatible are Core i 7 6700K (4.5 GHz) CPU, 32 GB of the memory and Windows 10 Pro OS. Furthermore, I ran the virtual computer VMware workstation

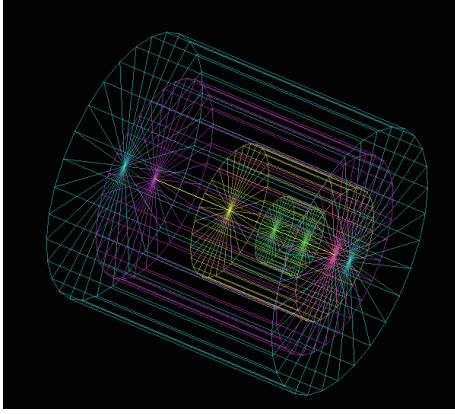


Figure 2: A state of executing the program `uclsource.f`. The region is all vacuum, the beam only fires straight. It does not count up. It is posted on the site [4].

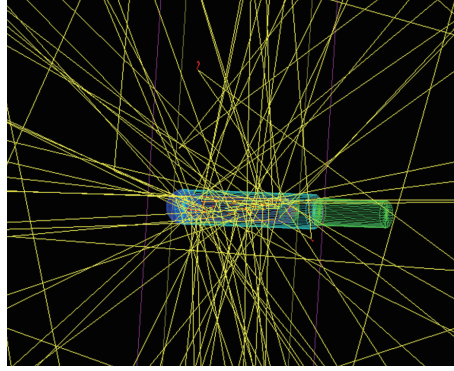


Figure 3: A state of executing the program of `test_small_Ir.f`. The radiation source is  $^{192}\text{Ir}$  microSelectron HDR-v2. The fine structure of the radiation source is also taken into consideration, and the absorbed dose is also aggregated according to the distance from the center of the source.

12.5.7 (4 core of CPU and memory use 4 GB) on Windows and ran Scientific linux Ver. 6.3 on it. When gfortran or g77 is used, it is confirmed that the calculation speed hardly changes on Windows or virtual computer. The results of the calculation time per core of Raspberry Pi and IBM PC compatible using these programs are shown in Fig.4 and Fig.5.

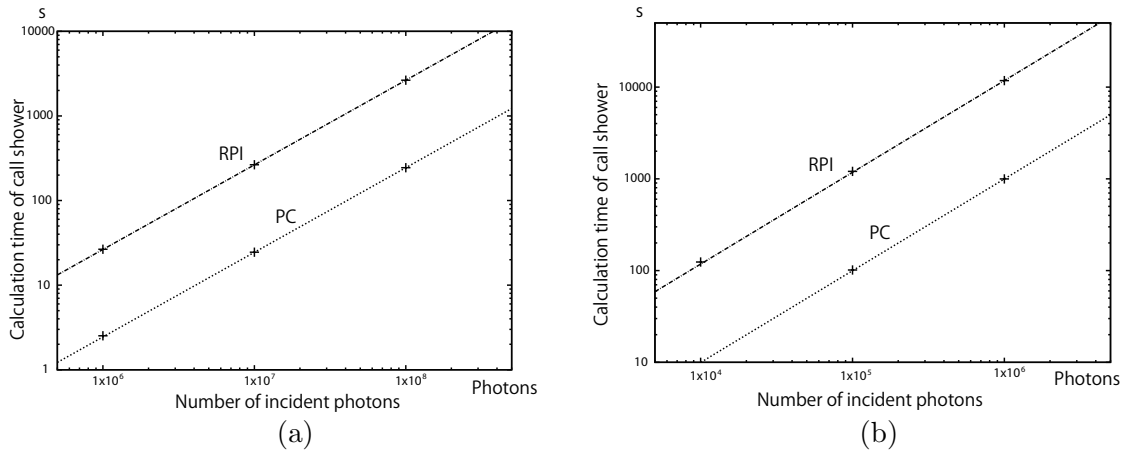


Figure 4: Calculation time of call shower. RPI: Raspberry Pi, PC: IBM PC compatible. (a) presents the result of `uclsource.f` and (b) presents `test_small_Ir.f`. The lines fit the plots.

The calculation time of Raspberry Pi is about 11 times ( $= 1/0.0897$ ) that of IBM PC compatible. In other words, Intel's Core i7 6700K is 11 times faster than the ARM Cortex-A 53. The ratio of calculation time did not change in either simple simulation (`uclsource.f`) or complicated simulation (`test_small_Ir.f`).

## 5 Calculation result with MPI

Raspberry Pi has 4 cores, so MPI can be run on one node. Fig.6 shows the ratio of the calculation results of single core and 4 cores when using `uclsource.f` and the improvement of `uclsource.f` for

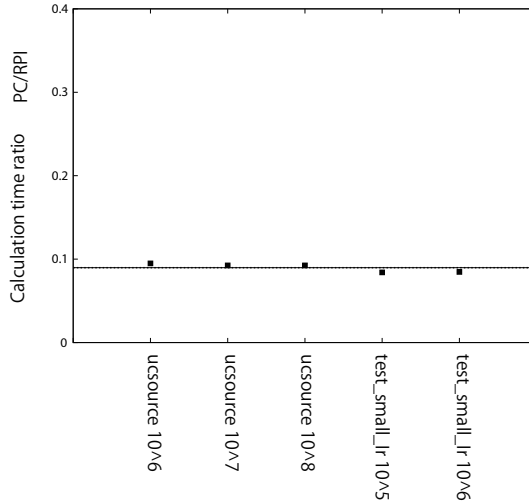


Figure 5: Calculation time ratio of Raspberry Pi and IBM PC compatible. RPI: Raspberry Pi, PC: IBM PC compatible. The straight line fitted the plot and the value was 0.0897.

MPI. The result of linear fitting the data was 0.239. This is approximately 1/4. When MPI is used

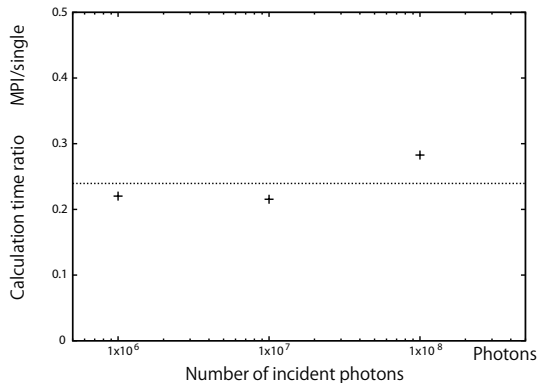


Figure 6: The ratio of the calculation results of single core and MPI (4 cores). The used programs are `ucsource.f` and the improvement of `ucsource.f`. The line fitted from the data shows 0.239.

with one node of Raspberry Pi, the calculation speed is 4 times faster than the single core. The value fitted to the data when using `test_small_lr.f` and the improvement of `test_small_lr.f` for MPI programs was 0.264, which was almost the same result. Note that the power consumption when calculating using 4 cores fully was about 4 W.

## 6 Other single board computers

Currently, besides Raspberry Pi, there are various single board computers. Among them, I report on the results of the investigation on BPI-M3 Banana Pi M3 and UDOO X86 Advanced Plus.

### 6.1 BPI-M3 Banana Pi M3

BPI-M3 Banana Pi M3 has A83T ARM Cortex-A7 Octa-core 1.8 GHz CPU, 2 GB memory and 8 GB flash eMMC. Compared to Raspberry Pi, a particularly prominent feature is having eight



cores in CPU.

## 6.2 UDOO X86 Advanced Plus

UDOO X86 Advanced Plus has Intel Celeron N3160 2.24 GHz CPU (4 cores) , 4 GB memory and 32 GB flash eMMC. A big difference from Raspberry Pi and Banana Pi is using an Intel processor instead of an ARM processor. In addition, it is possible to install ordinary Ubuntu or Windows 10 OS. UDOO X86 has a double area of the electronic circuit card compared to Banana Pi and Raspberry Pi.

## 6.3 Comparison of calculations between Raspberry Pi, Banana Pi and UDOO X86

Using MPI, we compared the computing capacity per board between Raspberry Pi, Banana Pi and UDOO X86. The number of CPU cores is 4 for Raspberry Pi, 8 for Banana Pi and 4 with UDOO X86. The programs used are the improvements of `ucsource.f` and the improvement of `test_small_Ir.f`. Fig. 7 shows the calculation results by MPI.

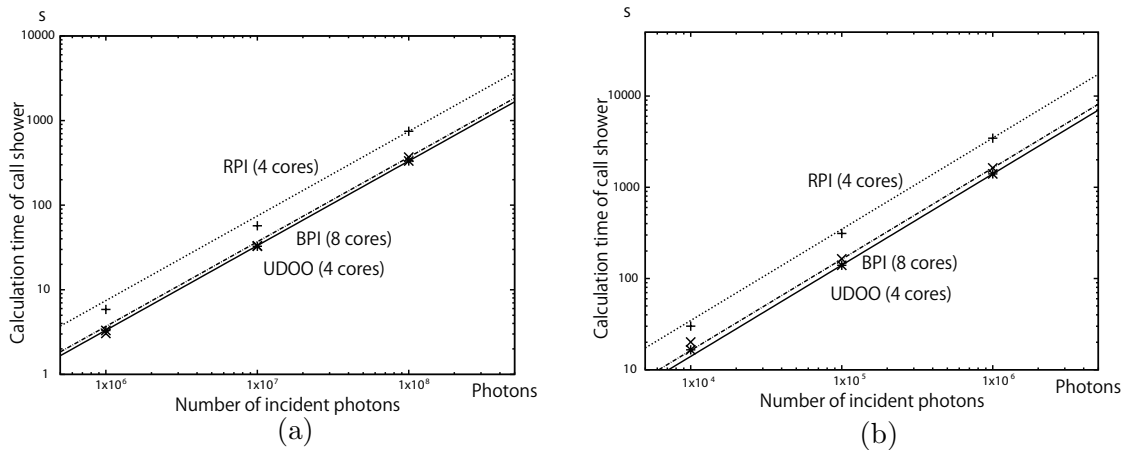


Figure 7: MPI calculation time of call shower. RPI: Raspberry Pi, BPI: Banana Pi, UDOO: UDOO X86. (a) presents the result of `ucsource.f` improvement for MPI and (b) presents `test_small_Ir.f` improvement for MPI. The lines fit the plots. The lines and plots represent the results of RPI, BPI, UDOO in order from the top.

The calculation time is UDOO X86 the earliest, but not so different from Banana Pi. It is almost the same as a simple program (improvement of `ucsource.f`), but there are slight differences in programs with complex processes (improvement of `test_small_Ir.f`). The ratios of computation time between single core and multiple cores with Banana Pi and UDOO X86 show approximately 1/8 and 1/4. The power consumption when Banana Pi calculated fully was about 5.2 W. With regard to UDOO X86, power consumption has not been investigated, but 12V 3A DC adapter is required.

## 7 Conclusion

I confirmed that EGS5 can be executed with Raspberry Pi 3 Model B. Furthermore, it was confirmed that EGS5-MPI can also be executed. I confirmed that EGS5 and EGS5 MPI also work on other single board computers, BPI-M3 Banana Pi M3 and UDOO X86 Advanced Plus. By combining a plurality of these single computers, it is possible to create a cluster computer of executing EGS5.

Among these, Banana Pi is most suitable for making cluster computers in terms of cost, power consumption, computing power and so on.

## References

- [1] <http://blog.shibayan.jp/entry/20150228/1425121187>, <https://jyn.jp/raspbian-setup/>.
- [2] H. Hirayama, Y. Namito, A.F. Bielajew, S. J. Wilderman and W. R. Nelson, "The EGS5 Code System," SLAC-R-730 (2005) and KEK Report 2005-8 (2005), <http://rcwww.kek.jp/research/egs/egs5.html>
- [3] M.Shimizu, EGS5-MPI, [https://unit.aist.go.jp/rima/ioniz-rad/egs5mpi/index\\_eng.html](https://unit.aist.go.jp/rima/ioniz-rad/egs5mpi/index_eng.html), [https://unit.aist.go.jp/rima/ioniz-rad/egs5mpi/doc/egs5mpi\\_manual\\_eng.pdf](https://unit.aist.go.jp/rima/ioniz-rad/egs5mpi/doc/egs5mpi_manual_eng.pdf).
- [4] <http://rcwww.kek.jp/research/egs/kek/egs5/uccg-150303.tar.gz>.
- [5] S.Tsuji, N.Narihiro, "ABOUT  $g(r)$  FUNCTION IN AAPM TG-43," Proceedings of the Eighteenth EGS Users' Meeting in Japan 6:36-42 (2011),  
S.Tsuji, N.Narihiro, "Comparison about Brachytherapy of Simulation EGS5 and Treatment Planning Based on AAPM TG-43," Proceedings of the Nineteenth EGS Users' Meeting in Japan 7:85-93 (2012)

# FOLLOW UP ON BETA RAY LIBRARY FOR EGS5

Y. Namito and H. Hirayama

KEK, Tsukuba 305-0801, Japan

## Abstract

We report the progress of the development of the beta ray energy spectrum library for EGS5. We examined numerical data of ICRU-56. Beta spectrum in Cross papers, ICRU 56, RADAR, ICRP 107 are compared.

## 1 Introduction

Since beta rays have a continuous energy distribution, energy distribution data and a sampling routine of energy using it are necessary for calculating beta rays with EGS5. Regarding the beta ray energy distribution, many studies have been conducted so far from both the theory and the measurement. Cross shows a figure of beta ray energy spectrum for 100 nuclides [1]. In ICRU Report 56, the numerical data shows the beta ray energy distribution per decay from representative 40 nuclides, and this is the most useful beta ray spectrum data collection [2]. In the ICRU Report 56, beta ray spectrum by Cross is shown as figures for 12 nuclides. The beta ray spectrum library RADAR [3] is published at Brookhaven National Laboratory. ICRP 107 Report [4] cover the beta ray spectrum from 1034 nuclides and are useful. Comparison of these databases or articles is shown in the table 1.

Table 1: Major beta ray spectrum library and paper

Title	Year	Number of nuclides	Energy points	Features
Cross	1983	100	–	Spectrum in figures. No numerical data
ICRU-56	1997	36	40	Figure from Cross and chart of unique calculation
RADAR	2002	429	20	Made and maintained at BNL
ICRP-107	2005	1034	~200	JAEA cooperates [5]

We have already made the energy distribution file of beta ray available in EGS5 code based on ICRU-56 and RADAR [6]. Beta libraries based on ICRP 107 are currently under construction. In this presentation, (1) Confirmation of contents of numerical data of ICRU-56 (2) Mutual comparison between ICRU-56, RADAR and ICRP 107 will be described.

## 2 Confirmation of contents of numerical data of ICRU-56

Table D.1 of ICRU-56 contains beta ray spectra from 40 nuclides. The first part of Table D.1 is written like the table 2, and the beta ray energy and the beta ray intensity are written. The value obtained by dividing the beta ray energy by the maximum beta ray energy is shown in the column titled as  $E/E_{\max}$ . When this is used for Monte Carlo calculation like egs5, it is necessary to set the energy section corresponding to the value of energy. As shown in Figure 1, one energy section is defined by the lower limit energy ( $E_{\text{low}}$ ) and the upper limit energy ( $E_{\text{up}}$ ), and its central energy ( $E_{\text{mid}}$ ) can also be considered.

Table 2: Part of Table D.1 (Beginning and ending of  $^{14}\text{C}$ ) data

$E/E_{\max}$	
0.000	1.549
0.025	1.594
0.050	1.690
—	—
—	—
0.950	0.016
0.975	0.004
1.000	0.000

Table 3: Treating "E in Table D1" as  $E_{\text{low}}$

$E_{\text{low}}/E_{\max}$	$E_{\text{up}}/E_{\max}$	
0.000	0.025	1.549
0.025	0.050	1.594
0.050	0.075	1.690
—	—	—
—	—	—
0.950	0.975	0.016
0.975	1.000	0.004
1.000	1.000	0.000

Table 4: Treating "E in Table D1" as  $E_{\text{mid}}$

$E_{\text{low}}/E_{\max}$	$E_{\text{up}}/E_{\max}$	
0.0000	0.0125	1.549
0.0125	0.0375	1.594
0.0375	0.0625	1.690
—	—	—
—	—	—
0.9375	0.9625	0.016
0.9625	0.9875	0.004
0.9875	1.0000	0.000

The problem here is that  $E$  shown in the table 2 corresponds to which of these three kinds of energy. One idea is that  $E$  matches  $E_{\text{low}}$ , in which case the table 2 is interpreted as table 3. The second idea is that  $E$  matches  $E_{\text{mid}}$ , in which case the table 2 is interpreted as table 4. If  $E$  matches  $E_{\max}$ , the first value (1.549) of the spectrum corresponds to negative energy, which is obviously wrong, so in this case exclude.

We will investigate which of these two ideas is appropriate for the following three items. The beta ray intensity per decay is shown in Figure 2. The value of the idea of  $E_{\text{mid}}$  well matches RADAR and ICRP 106, whereas the value of  $E_{\text{low}}$  is out of consideration. For this reason, the idea of  $E_{\text{mid}}$  is supported as the first clue.

Next, we compare the beta-ray spectrum. For example, if we plot with the idea of  $E_{\text{mid}}$  as shown in Figure 3, it is close to the spectrum of Cross. From this point,  $E_{\text{mid}}$  is supported rather than  $E_{\text{low}}$ . Furthermore, the average energy of the beta ray is shown in Fig. 4. Since the average energy calculated based on  $E_{\text{mid}}$  well matches the value of Cross,  $E_{\text{mid}}$  is supported.

As a result, the following conclusions are obtained from all three comparisons.

- The energy in Table D.1 shows the energy at the center of each energy bin and the table 2 is interpreted like the table 4.

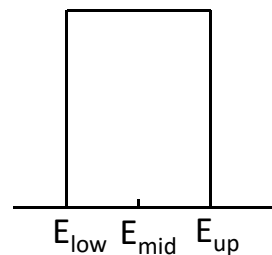


Figure 1: Relation of  $E_{\text{low}}$ ,  $E_{\text{mid}}$ , and  $E_{\text{up}}$

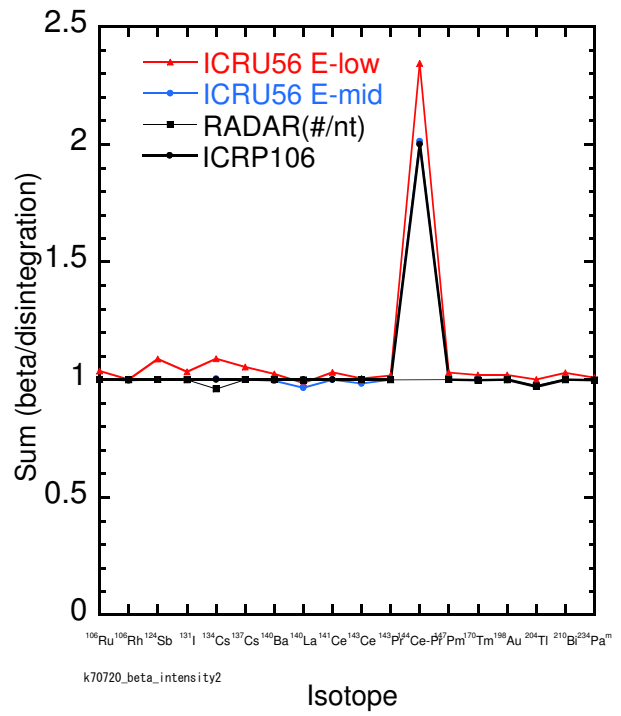
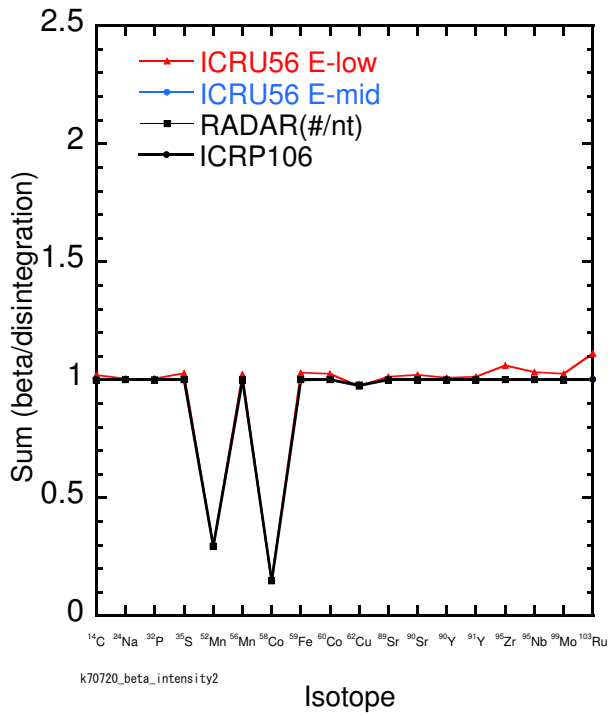


Figure 2: Comparison of beta intensity

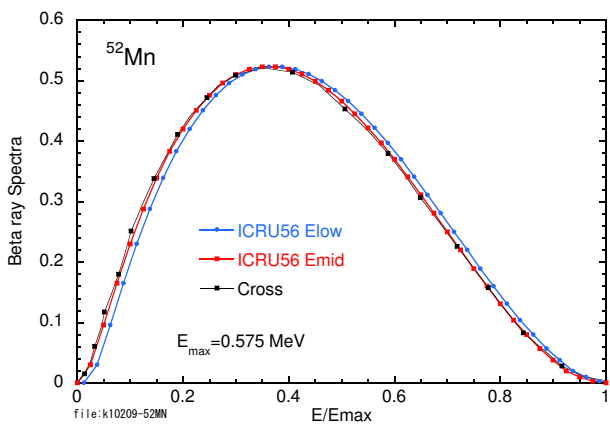


Figure 3: Comparison of beta spectra from Mn-52

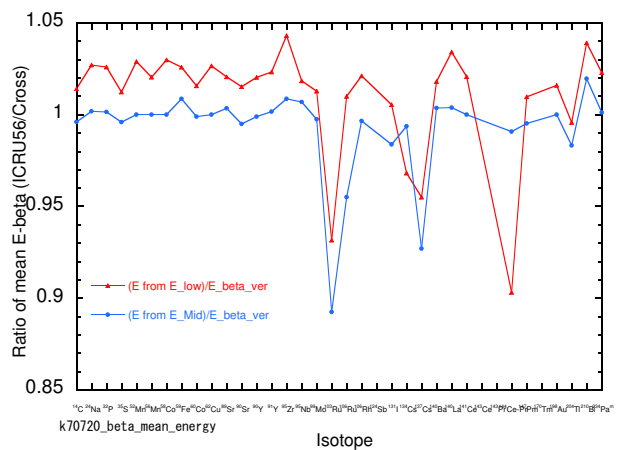


Figure 4: Comparison of beta ray mean energy

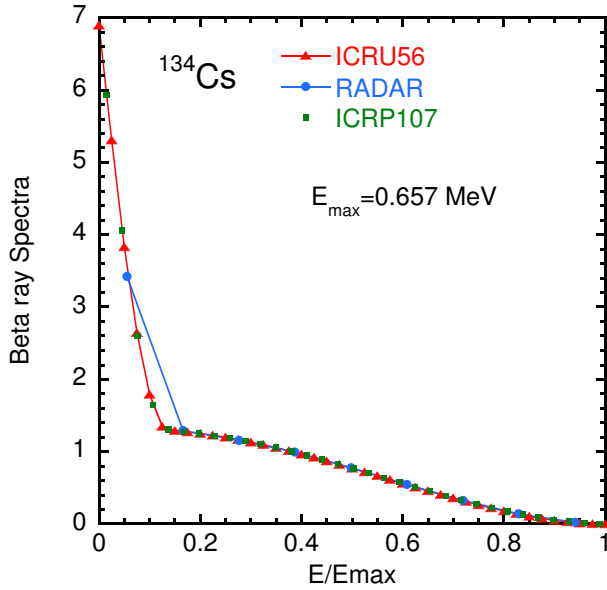


Figure 5: Comparison of beta spectrum from  $^{134}\text{Cs}$

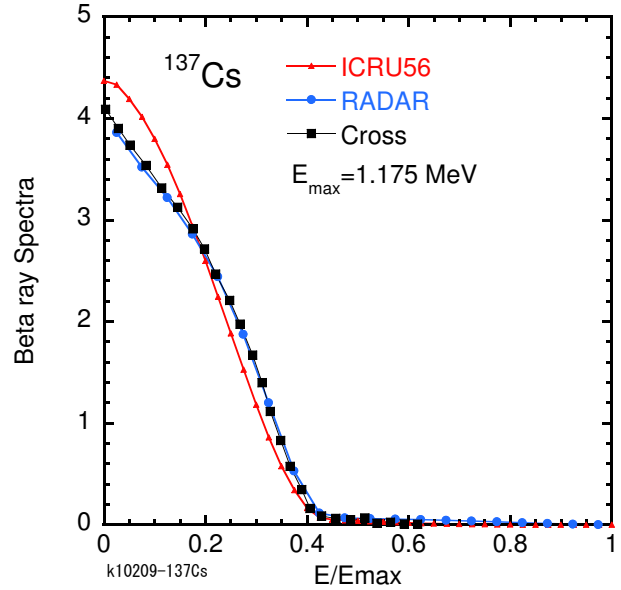


Figure 6: Comparison of beta spectrum from  $^{137}\text{Cs}$

### 3 Comparison of ICRU 56, RADAR, ICRP 107

Beta ray spectra of ICRU-56, RADAR, ICRP-107, Cross are compared. In many nuclides, spectra from different databases agreed well. Here, there was a significant difference depending on the database for  $^{134}\text{Cs}$  (Fig. 5),  $^{137}\text{Cs}$  (figure 6),  $^{204}\text{Tl}$  (figure 7),  $^{210}\text{Bi}$  (figure 8). For  $^{134}\text{Cs}$ , RADAR is different from ICRU-56 and ICRP107 at low energy. This is due to the fact that the number of energy divisions of RADAR is as small as 20 points. Since the difference is limited to the low energy part, this difference can be ignored if the low energy part is not important. For  $^{137}\text{Cs}$ , JAERI 1357 criticizes that use of form factor of allowable transition in ICRU-56 is not appropriate.

For  $^{204}\text{Tl}$ , Cross and ICRU 56, RADAR and ICRP-107 agree well, respectively, and the former emphasized agreement with the experiment and it is a calculation by using empirical form factor. Also for  $^{210}\text{Bi}$ , Cross and ICRU-56 and RADAR and ICRP-107 agree well, respectively. Cross adopted the experimental value, ICRU-56 is calculation by form factor adjusted to fit the experiment. The user decides which data to use for these nuclides. If emphasis is placed on agreement with the experimental value in ICRU-56 is a good choice.

Beta ray spectra of ICRU-56, RADAR, ICRP-107 are summarized. Points to keep in mind about ICRU-56 data are as follows.

1. The spectrum of  $^{137}\text{Cs}$  in ICRU-56 is different from other data. It seems to be due to the fact that shape factors different from other data are used.
2. For  $^{204}\text{Tl}$  and  $^{210}\text{Bi}$ , shape factors adjusted was used to reproduce the experimental values well, which is useful for comparison with experiments on these nuclides.

Points to keep in mind about RADAR data are as follows.

1. Most of the nuclides are in good agreement with ICRU-56. In other words, nuclides contained in both ICRU-56 and RADAR and other than the above three nuclides can use either data.
2. The energy score is as small as 20. In the low energy part of  $^{134}\text{Cs}$ , this gives rise to a certain degree of spectral error.

A summary of ICRP-107 is as follows.

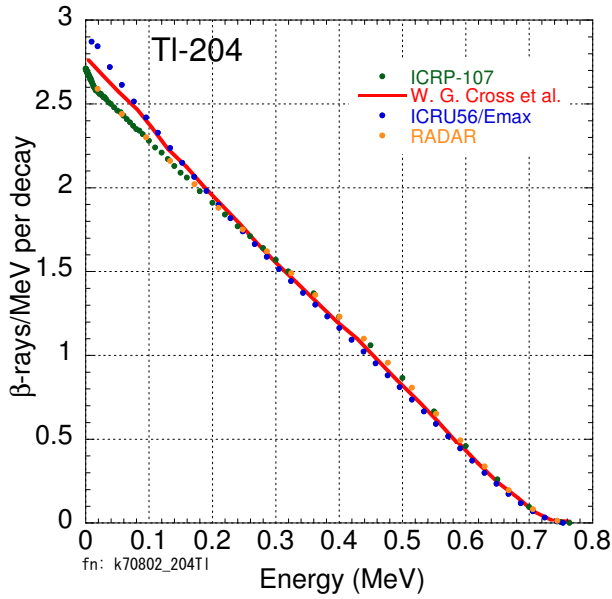


Figure 7: Comparison of beta spectrum from  $^{204}\text{Tl}$

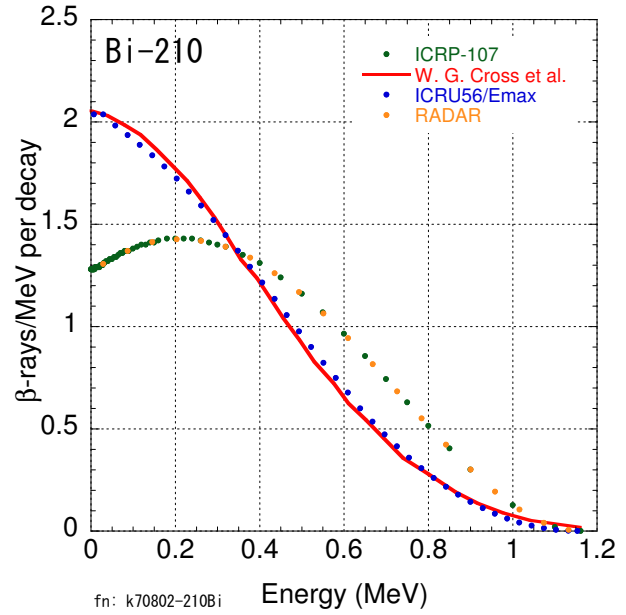


Figure 8: Comparison of beta spectrum from  $^{210}\text{Bi}$

1. For slight nuclides comparing spectra, it agreed well with RADAR.
2. We are promoting maintenance of the input file of EGS5 and are scheduled to be released soon.

## References

- [1] W. G. Cross, H. Ing, and N. O. Freedman, “A short atlas of beta-ray spectra”, *Phys. Med. Biol.* **28**, 1251-1260 (1983).
- [2] “Dosimetry of External Beta Rays for Radiation Protection”, ICRU Report 56 (1997).
- [3] <http://www.doseinfo-radar.com/RADARDecay.html> (2017.09.12 final confirmation)
- [4] “Nuclear Decay Data for Dosimetric Calculations”, ICRP Publication 107, *Annals of ICRP*, 38 (2008).
- [5] A. Endo, Y. Yamaguchi and K. F. Eckerman, “Nuclear Decay Data for Dosimetry Calculation Revised Data of ICRP Publication 38”, JAERI 1347, Japan Atomic Energy Research Institute (2004).
- [6] Y. Kiriara, H. Hirayama and Y. Namito, “ $\beta$ -ray Spectrum Data for egs5 based on ICRU-56 or RADAR”, KEK Report 2016-2, KEK (2016).

# EVALUATION OF MULTI-LAYERED SHIELDING MATERIALS BASED ON ANALYSIS OF CHARACTERISTIC X-RAY

**D. Kawahara, T. Tobusawa, N. Sakurai**

*Tokyo Metropolitan Industrial Technology Research Institute, Tokyo 135-0064, Japan  
e-mail: kawahara.daigo@iri-tokyo.jp*

## **Abstract**

Non-lead materials are spread for materials of protective devices against diagnostic X-ray. The relationships between X-ray energy and protective performances of the non-lead materials, as lead equivalent, are complex because of photoelectric effect by white X-ray. In this study, the ratios of the characteristic X-ray into transit X-ray through protective materials were calculated with Monte-Carlo simulation code EGS5 and measured with CdTe semiconducting detector respectively, based on the narrow beam condition of JIS Z 4501. Additionally, the bi-layer materials consisted of low density and high density materials were designed and evaluated their availability.

## **1. Introduction**

Generally protective aprons for diagnostic X-ray were required protective performance of equivalent to 0.25 mm thickness Pb. And non-lead materials used for X-ray protective aprons and other devices achieved in international demands to lead free products. X-ray protective performances of non-lead materials, such as lead equivalent, depend to X-ray energy. These dependants are due to different in photoelectric effect and scattered photon between lead and non-lead materials. Since medical exposures are increasing with the growth of CT, IVR [1], and so on, evaluation of protective performances against X-ray in their techniques are important. The performances of protective devices are evaluated from dose with imaging plates [2], and effective energy with CdTe semiconducting detector [3]. However, X-ray energy-dependency of protective performances as lead equivalent did not study with detail evaluation of their interaction as photoelectric effect.

In this study, we evaluated X-ray transmission rates and ratios of characteristic X-ray as protective performances of lead and non-lead materials based on method in JIS Z 4501, numerically with EGS5 code (a simulator that performs transport calculation by the Monte Carlo method) and experimentally with CdTe semiconducting detector.

## **2. Numerical experiment**

### **2.1 Geometry of simulation**

For source data of simulation, distribution of X-ray energy in tube voltage 100 kV and total filtration of 0.25mm Cu is measured at 0.5 keV intervals with CdTe semiconducting detector. The point source is set to 1500 mm from specimens and limit X-ray beam to angle as cut detector side surface of specimens to 20 mm in diameter according to setting of narrow beam condition in JIS Z 4501 (Figure1). The number of photon is set to  $10^7$ . The detector is set to 50 mm behind from specimens in the direct line through source and specimens. Area of detector is  $4 \times 4 \text{ mm}^2$ .

### **2.2 Specimens**

Barium sulfate specimens of thickness 0.1mm (Ba01), 0.6 mm (Ba06), 2.0 mm (Ba2), and bi-layered specimens consist of 0.1 mm thickness barium sulfate and 0.1 mm thickness tungsten that barium sulfate set to source side



(Ba01W01), and tungsten is source side (W01Ba01) are used. The areas of specimens are 100 x 100 mm<sup>2</sup>.

### **2.3 Evaluation of protective performances**

On the detector surface, doses of X-ray without specimens and transit dose with specimens were measured and calculate transmission rate of X-ray through specimens.

The net areas of peaks of characteristic X-ray of barium and tungsten were calculated as characteristic X-ray doses from distribution of energy of transited X-ray through specimens. The net areas are measured as product of peak height and full width at half maximum, FWHM. The ratios of characteristic X-ray doses from specimens to transit doses through specimens are calculated.

## **3. Experiments**

### **3.1 Geometry of simulation**

Energy spectrums of X-ray transited through materials are measured with CdTe semiconducting detector. X-rays were radiated at tube voltage 100 kV and total filtration 0.25 mm Cu with tungsten target X-ray generator MG452 (YXLON International K.K.), and were measured with CdTe semiconducting detector SCT404005 and pre-amp type-579 (CLEAR-PULSE Co., Ltd.). CdTe element size was 4 x 4 mm<sup>2</sup> and 0.5 mm thickness.

The specimens were set to 1500 mm from focus generated X-ray, and the detector was set behind specimens to 50 mm. The collimator of 10 mm thickness lead with aperture of 15 mm diameter was set to 200 mm front of specimens (Figure1), and the collimator consisted of 5 mm thickness lead and 1 mm copper with aperture of 1 mm diameter was set close to the detector.

### **3.2 Specimens**

Barium sulfate dispersed gum sheets and tungsten board (Rare Metallic Co., Ltd.) are used in the size of 10 x 10 mm<sup>2</sup>. The gum sheets are based on EPDM base gum (Takehara Rubber Co., Ltd.), and were dispersed barium sulfate powder (Wako) equivalent weight of board with 0.1 mm thickness, 2.0mm thickness, and were vulcanized. The EPDM gum base compound from EPDM 100, oil 70, silica 70 with ratio by weight, and add sulfur (Hosoi Chemical Industry Co., Ltd.) as cross-linker, rubber antioxidant, vulcanization accelerator, process aid, and anti-cracking agents.

### **3.3 Evaluation of protective performances**

Spectrum of X-rays without specimens and transit doses with specimens were measured and calculate transmission rate of X-ray through specimens. Their X-ray photons were measured and discriminated their energy with portable multichannel analyzer ORTEC DART (AMETEK, Inc.) during 300 sec without dead time of measurement kept under 10%.

The net areas of peaks of characteristic X-rays of barium and tungsten were calculated as the characteristic X-ray doses from distribution of energy of transited X-ray through specimens. Net areas are measured as product of peak height and full width at half maximum, FWHM. The ratios of characteristic X-ray doses from specimens to transit doses through specimens are calculated.

## **4. Results**

Figure2 shows X-ray transmission rates of specimens calculated by EGS5 simulations and measured with CdTe semiconducting detector. The barium sulfate specimens increased in the X-ray transmission rates with increase in their thickness, and shows consistent values between analytical values and experimental values. X-ray transmission rates of bi-layered specimens consisted of 0.1 mm barium sulfate and 0.1 mm tungsten are nearly equal to it of 0.6 mm barium sulfate, and the smallest transmission rate is shown by bi-layered specimen set barium sulfate to source side.

Figure 3 shows the ratios of characteristic X-ray doses to transit X-ray doses calculated and measured. The barium sulfate specimens increased in the ratio of characteristic X-ray of barium sulfate, but were approximately consistent in the ratio of characteristic X-ray of tungsten with increase in their thickness. The bi-layered specimens were decreased in the ratios of characteristic X-ray of barium sulfate to nearly them in the case of without specimens, but were increased in the ratio of characteristic X-ray of tungsten 2 to 4 times against them of the barium sulfate specimens. The bi-layered specimen set barium sulfate to source side was smaller in the ratio of characteristic X-ray doses of barium sulfate and larger in the ratio of the characteristic X-ray doses of tungsten than the specimen set tungsten to source side.

## 5. Discussion

It is known that X-ray transmission rates with 100 kV tube voltage X-rays through 0.25 mm Pb measured with conditions based on JIS Z 4501 is approximately 0.2.

In this study, the specimens of 0.6 mm barium sulfate, and bi-layered specimens consisted of 0.1 mm barium sulfate and 0.1 mm tungsten showed approximately 0.2 of X-ray transmission rates with 100 kV tube voltage condition. And weight per area in 100 x 100 mm<sup>2</sup> specimens of 0.6 mm barium sulfate and bi-layered specimens were 0.270 g/cm<sup>2</sup>, 0.238 g/cm<sup>2</sup>, respectively, and smaller than them of 0.25 mm Pb (0.284 g/cm<sup>2</sup>) by 5%, 17% respectively. The barium sulfate specimens increased in the ratios of characteristic X-rays of barium to transit X-rays with increase in their thickness. It is considered that the transit X-rays decreased with increasing of thickness of material, and the characteristic X-rays of barium emitted at nearly surface of detector side were little attenuated. However ratios of the characteristic X-rays of tungsten were approximately consistent with increasing of thickness of materials. It is considered that the characteristic X-rays of tungsten were only emitted at focus of X-ray tube, and attenuated by specimen as with other X-rays from source.

The bi-layered specimens were smaller in the ratios of characteristic X-rays of barium, and larger in the ratios of characteristic X-rays of tungsten than the barium sulfate specimens, if bi-layered specimens were set the tungsten layer to each of source side and detector side. It is considered that the characteristic X-ray of barium had low energy comparatively (36.4, 32.2 keV) and attenuated by tungsten set to detector side, or their emitting were decreased by attenuation of X-ray of energy used for photoelectric effect of barium. Otherwise, the characteristic X-rays of tungsten (67.2, 59.3 keV) from bi-layered specimens were difficult to attenuate by barium sulfate set to detector side if tungsten set to source side, and decreasing their emitting by attenuation of X-rays of energy used for photoelectric effect of tungsten was difficult to barium sulfate set to source side.

The ratios of characteristic X-rays of tungsten from bi-layered specimens were different between calculated and measured. It may be attributed that the thickness of element of CdTe semiconducting detector was not enough to absorb all of X-ray, or details of base materials used for experiments were not enough calculated.

The narrow beam condition defined on JIS Z 4501 is basically made to estimate attenuation of X-ray by shielding materials without secondly X-ray including scattering X-ray and characteristic X-ray, but effects from characteristic X-ray are not completely removed because they emitted isotropically freely from energy dependence of incident X-ray. Thus, the ratios of characteristic X-ray from materials or source increase with decreasing of transit X-ray. In this study, multi-layered shielding materials were attenuated effectively to attenuate the characteristic X-rays of light material by heavy material set to detector (patients or operator side during diagnosis). But the characteristic X-ray from heavy material and source are only little attenuated. It is considered that lighter materials than tungsten are suitable as heavy materials of bi-layered shielding materials to attenuate the characteristic X-rays from their and source effectively.

## 6. Conclusions

Lead equivalent is one of the standards of performance for protective devices against diagnostic X-ray, and 0.25 mm Pb is typically required. This lead equivalent value means that X-ray transmission rate is almost 0.2 against X-ray emitted with

100kV tube voltage based on the narrow beam condition of JIS Z 4501. In this study, 0.6mm barium sulfate specimen and bi-layered specimens consisted of 0.1 mm barium sulfate and 0.1 mm tungsten indicated almost equal in X-ray transmission rate to 0.25 mm Pb. Additionally, The area densities of these non-lead specimens were lower than the area density of 0.25 mm Pb. Their results indicate that non-lead specimens protect X-ray effectively in this condition.

The barium sulfate specimens were increased in the ratios of the characteristic X-ray of barium to transit X-ray with the increase in their thickness and protective performance. On the other hand, the multi-layered specimens were decreased in the ratios of the characteristic X-ray of barium to transit X-ray and were nearly equal to value in the case of without specimens. Thus, multi-layered materials show effective protecting to X-ray with attenuation or prevention of the characteristic X-ray from low density materials. However, the multi-layered specimens were increased in the ratios of the characteristic X-ray of tungsten. It is considered that lighter materials than tungsten are suitable as heavy materials of bi-layered shielding materials to attenuate the characteristic X-rays from their and source effectively.

## References

- 1) S. Power, M. Mirza, A. Thakorlal, B. Ganai, L. D. Gavagan, M. F. Given, M. J. Lee: "Efficacy of a Radiation Absorbing Shield in Reducing Dose to the Interventionalist During Peripheral Endovascular Procedures: A Single Centre Pilot Study", *Cardiovasc Intervent Radiol*, **38**, 573-578 (2015)
- 2) H. Miyamaru, I. Murata, R. Taniguchi, H. Shimomura and S. Okuda: "Gamma-ray Transmission Evaluation using Imaging Plate Designed for X-ray Radiography", *Prog. Nucl. Sci. and Tec.*, **4**, 699-703 (2014)
- 3) J.C. Santos, P.R. Costa: "Evaluation of the Effective Energy of Primary and Transmitted Workload Weighted X-ray Spectra", *Rad. Phys. and Chem.*, **95**, 221-223 (2014)

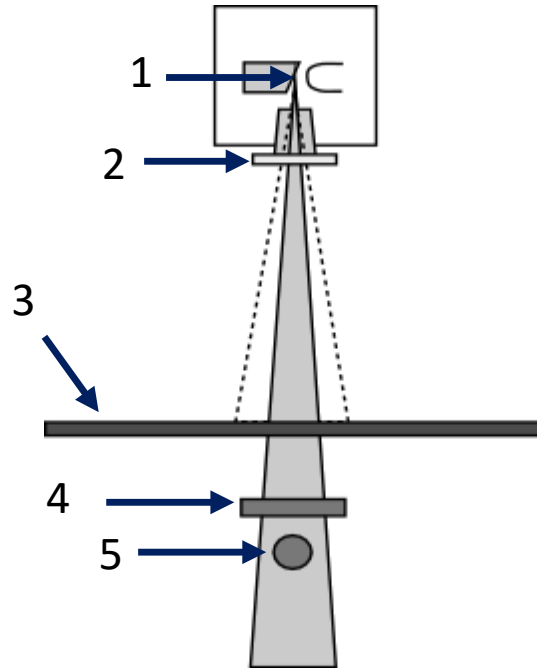


**Figure 1.** Narrow beam condition in JIS Z 4501  
 (1: focus, 2: additional filter, 3: collimator, 4: specimen, 5: detector)

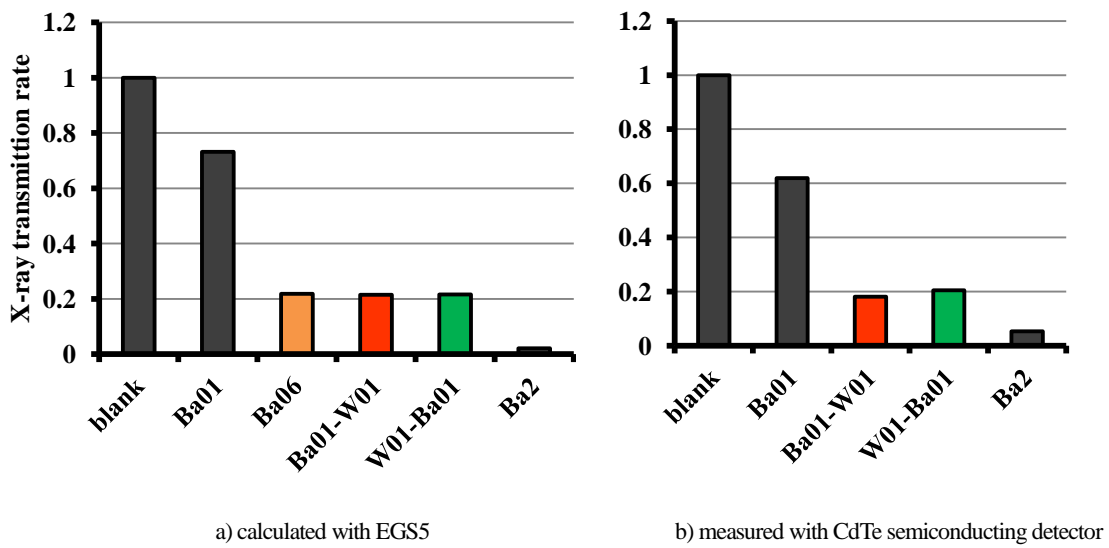
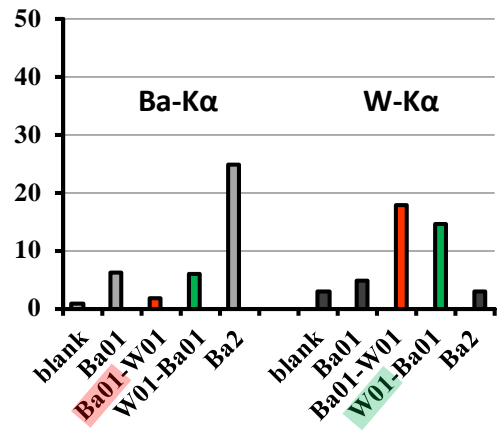
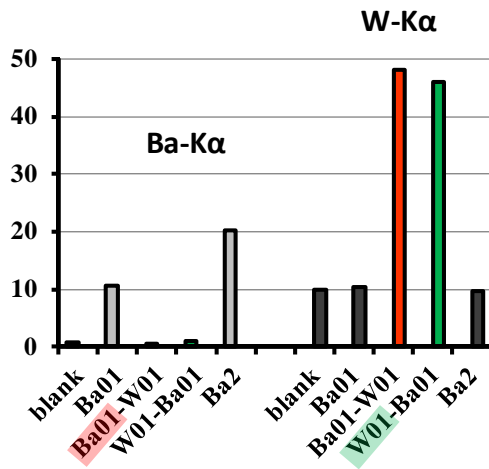


**Figure 2.** X-ray transmission rate against X-ray of 100 kV tube voltage

The ratios of the characteristic X-rays  
to transit X-rays



a) calculated with EGS5

b) measured with CdTe semiconducting detector

**Figure 3.** The ratios of the characteristic X-rays from specimens to transit X-rays